Reactivities of Interstitial Hydrides in a Cu-11 Template: En Route to Bimetallic Clusters

Rhone P. Brocha Silalahi, Qi Wang, Jian-Hong Liao, Tzu-Hao Chiu, Ying-Yann Wu, Xiaoping Wang, Samia Kahlal, Jean-Yves Saillard, C. W. Liu

10.1002/anie.202113266

WILEY-VCH

RESEARCH ARTICLE

Reactivities of Interstitial Hydrides in a Cu_{11} Template: En Route to Bimetallic Clusters

Rhone P. Brocha Silalahi,[a] Qi Wang,[b] Jian-Hong Liao,[a] Tzu-Hao Chiu,[a] Ying-Yann Wu,[c] Xiaoping Wang,[d] Samia Kahlal,[b] Jean-Yves Saillard,[b]* and C. W. Liu*[a]

[a] Dr. R. P. B. Silalahi, Dr. J.-H. Liao, T.-H. Chiu, Prof. Dr. C. W. Liu
Department of Chemistry, National Dong Hwa University
No. 1, Sec 2, Da Hsueh Rd., Hualien 974301, Taiwan (R. O. C.)
E-mail: chenwei@mail.ndhu.edu.tw
Homepage: http://faculty.ndhu.edu.tw/~cwl/index.html
[b] Dr. Q. Wang, Dr. S. Kahlal, Prof. Dr. J. -Y. Saillard
Univ Rennes, CNRS, ISCR-UMR 6226
F-35000 Rennes, France
[c] Dr. Y.-Y. Wu
Institute of Chemistry, Academia Sinica,
Taipei 11528, Taiwan (R. O. C.)
[d] Dr. X. P. Wang
Neutron Scattering Division, Neutron Sciences Directorate, Oak Ridge National Laboratory,
Oak Ridge, TN 37831, U.S.A.

Supporting information for this article is given via a link at the end of the document

Abstract: In sharp contrast to that of surface hydrides, reactivities on interstitial hydrides are difficult to explore. When treated with a metal ion (Cu^+, Ag^+, and Au^+), the stable Cu(I) dihydride template $[Cu_{11}H_2\{S_2P(O^iPr)_2\}_6(C{\equiv}CPh)_3]$ (**H_2Cu_{11}**) generates surprisingly three very different compounds; namely $[CuH_2Cu_{11}\{S_2P(O^iPr)_2\}_6(C{\equiv}CPh)_3]^+$ (**1**), $[AgH_2Cu_{14}\{S_2P(O^iPr)_2\}_6((C{\equiv}CPh)_6]^+$ (**2**), and $[AuCu_{11}\{S_2P(O^iPr)_2\}_6(C{\equiv}CPh)_3Cl]$ (**3**). **1** and **2** are both M(I) species and maintain the same number of hydride ligands as their **H_2Cu_{11}** precursor. Neutron diffraction revealed the first time a trigonal pyramidal hydride coordination mode in an $AgCu_3$ environment of **2**. The bimetallic cluster of **3** has no hydride and exhibits a mixed-valent $[AuCu_{11}]^{10+}$ metal core, making it a 2-electron superatom. Thus, depending on the nature of M^+, trigonal pyramidal hydrides of the **H_2Cu_{11}** reactant behave differently. In the cases of M = Cu or Ag, they act as regular 2-electron ligands. In the case of M = Au, they behave as electron donors, leading to the formation of a 2-electron superatom, with liberation of H_2.

Introduction

Coinage metal hydride nanoclusters (NCs) are currently of a foremost interest, owing to their unique and extensive structural and bonding features, broad applications in catalytic reactions, and potential use in the design of hydrogen storage materials.[1-3] In the past, our group reported the composition, structure (including neutron diffraction analysis), and electronic properties of copper(I) hydrides. Notable examples are dithiocarbamate(dtc)-stabilized Cu_7H and $Cu_{28}H_{15}$,[4-5] dithiophosphate(dtp)/diselenophosphate(dsep)-protected $Cu_{20}H_{11}$,[2a, 6] $Cu_{30}H_{18}$,[7] and $Cu_{32}H_{20}$.[8] In these copper(I) NCs, the hydrides are clearly hydridic as they react with protons of terminal alkynes to yield medium-sized, dtp (or dtc)/alkynyl-protected $Cu_{11}H_2$,[9] and -$Cu_{15}H_2$.[10] At the same time, we explicitly demonstrated by spectroscopy that the hydrides in $Cu_{15}H_2$ are able to reduce Cu(I) to Cu(0) from which a Cu-centered Cu_{12} cuboctahedral $[Cu_{13}(dtc)_6(C{\equiv}CPh)_4]^+$,[11] a two-electron superatom, was formed.[10]

Another well-established reaction in these copper hydrides is the controlled synthesis of alloy clusters via doping the dichalcogenolate-stabilized copper hydrides with group 10 heterometals. In that respect, the reaction of $[Cu_{28}H_{15}(S_2CN^nBu_2)_{12}]^+$ or $[Cu_{20}H_{11}\{S_2P(O^iPr)_2\}_9]$ with phenylacetylene in the presence of $Pd(PPh_3)_2Cl_2$ generates $[PdH_2@Cu_{14}(dtc/dtp)_6\{C{\equiv}CPh\}_6]$ ($Cu_{14}PdH_2$),[7,12] *the first examples of structurally precise copper clusters doped with palladium group metals*. The two hydrides are strongly bonded to Pd in a linear fashion, supporting the view of a 14-electron $[PdH_2]^{2-}$ unit encapsulated in a $[Cu_{14}]^{14+}$ cage. In fact, the neutral $Cu_{14}PdH_2$ alloy molecules are iso-structural with the $Cu_{15}H_2$ monocations. By using the reducing power of the hydrides, it is also possible to synthesize the 2-electron bimetallic superatoms $[M@Cu_{12}(dtp)_6(C_2Ph)_4]^+$ (M = Ag, Au) via heterometal-doping onto copper hydrides.[13]

These studies allow envisioning new synthetic strategies in producing mono- and bimetallic-Cu-rich hydrides and the growth of nanoscale copper clusters. They seamlessly contribute to the topical field of alloy NCs,[14] a class of compounds which allows to modify optical properties, enhance the stability, and tune the photoluminescent performance compared to their homometallic relatives. However, the coordinated hydrides within homometallic copper NCs have never been used as ligands in the formation of heterometallic derivatives, except perhaps in the case of $Cu_{14}PdH_2$.[7,12] In sharp contrast, M-H-M' fragments are frequently observed in metal hydrides, depicting donor-acceptor relationships.[15] Surprisingly, such hydride-bridged, heterometallic clusters were predominantly formed via the coordinating ability of surface hydrides. *Never have interstitial hydrides behaving as Lewis bases been observed in heterometallic clusters*, to the best of our knowledge.

We recently reported the synthesis, structure, and optical properties of a heteroleptic Cu_{11} cluster, $[Cu_{11}H_2\{S_2P(O^iPr)_2\}_6(C{\equiv}CPh)_3]$ (**H_2Cu_{11}**),[9] which contains two

encapsulated hydrides, each in trigonal pyramidal geometry. Potentially the μ4-hydrides in **$Cu_{11}H_2$** may exhibit dual functions, that of ligands and that of reductants. Herein we report the synthesis and crystal structures of mono and bimetallic copper-rich NCs: $[Cu_{12}H_2\{S_2P(O^iPr)_2\}_6(C{\equiv}CPh)_3]^+$ (**1**); $[AgH_2Cu_{14}\{S_2P(O^iPr)_2\}_6(C{\equiv}CPh)_6]^+$ (**2**), and $[AuCu_{11}\{S_2P(O^iPr)_2\}_6(C{\equiv}CPh)_3Cl]$ (**3**) for which the hydrides act as Lewis bases during the synthesis of **1** and **2**, but as reductants in that of **3**. Furthermore, the degradation of **2** and partial aggregation of **3** in solution reveal that bimetallic clusters **2** and **3** are key precursors en route to the more stable 2-electron superatomic alloys, $[M@Cu_{12}\{S_2P(O^iPr)_2\}_6(C{\equiv}CPh)_4]^+$ (M =Au, **4**; Ag, **5**).[13] Intriguingly, the metal core of **3**, which can be best described as a vertex-missing Au-centered Cu_{12} cuboctahedron, displays an *fcc* structure with a vacancy defect, which is closely related to that of **4**, a full *fcc* array. Thus, the first two-electron superatomic alloy with a defect *fcc* lattice is revealed in **3**.

Results and Discussion

Synthesis and Characterizations

The reaction of **H_2Cu_{11}** with $[Cu(CH_3CN)_4](PF_6)$ in a 1:1 molar ratio at ambient temperature in acetone produces within 10 minutes an orange precipitate of $[CuH_2Cu_{11}\{S_2P(O^iPr)_2\}_6(C{\equiv}CPh)_3]^+$ (**1_H**) in 95% yield (Scheme 1). An alternative synthetic procedure can be conducted through a one-pot synthesis method in which $[Cu(CH_3CN)_4](PF_6)$ and $[NH_4][S_2P(O^iPr)_2]$ are dissolved in a 1/1 mixture of CH_3CN and THF, followed by the addition of HC≡CPh and Et_3N. After 10 minutes, $NaBH_4$ is added quickly. The mixture continues stirring at 32° for 3 hours. A workup of this mixture affords cluster **1_H** in 28.2% yield. The corresponding deuteride derivative $[CuD_2Cu_{11}\{S_2P(O^iPr)_6\}_2(C{\equiv}CPh)_3]^+$ (**1_D**) was synthesized to support the existence of two hydride ligands, which were confirmed by ^2H NMR spectroscopy.

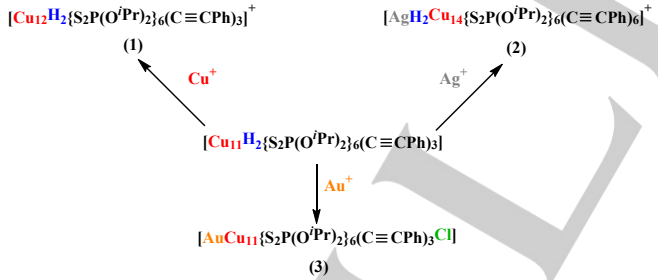

Scheme 1. The synthesis of compounds **1**, **2**, and **3** from the **H_2Cu_{11}** template.

The composition of **1_H** was first determined by positive-ion ESI-MS spectrometry. The spectrum of **1_H** depicts prominent peaks at *m/z* 2346.41 (calc. 2346.38) and *m/z* 2283.48 (calc. 2283.45), corresponding to the molecular cation of **$[1_H]^+$** and the neutral template **[H_2Cu_{11}]**, respectively (Figure S1). Their simulated isotopic patterns are in good resemblance with their experimental counterparts (Figure S1: inset). The ESI-MS analysis of the deuteride analogue (**1_D**) depicts a similar pattern with peaks at *m/z* 2348.37 (**$[1_D]^+$**, calc. 2348.40), and 2285.45 (**D_2Cu_{11}**, calc. 2285.47) (Figure S2). The exact two mass unit difference between **1_H** and **1_D** confirms the existence of two hydrides.

NMR spectroscopy is quite diagnostic of the insertion of a copper atom into the **H_2Cu_{11}** template. The resonances of the phenyl protons and hydrides are shifted downfield from 7.32-7.68 to 7.46-7.74 ppm (Figures S3 and S4) and from 4.89 (**H_2Cu_{11}**) to 5.24 ppm (**1_H**) (Figure S5), respectively. The deuteride resonance of **1_D** in acetone shows a single peak at δ = 5.29 ppm in the ^2H NMR spectrum (Figure S5). The phosphorus resonance of the dtp ligands in **1_H** displays an up-field shift to 99.5 ppm from 104.2 ppm in **H_2Cu_{11}**.

To prepare $[AgH_2Cu_{14}\{S_2P(O^iPr)_2\}_6(C{\equiv}CPh)_6]^+$ (**2_H**), one equiv. of $[Ag(CH_3CN)_4](PF_6)$ was added into **H_2Cu_{11}** acetone solutions at ambient temperature for 10 minutes. Purification of the crude products yields black residues in a 24.6% yield (Scheme 1). To support the existence of two hydrides in the cluster, the deuteride analogue $[AgD_2Cu_{14}\{S_2P(O^iPr)_2\}_6(C{\equiv}CPh)_6]^+$ (**2_D**) conducted by a similar synthetic procedure was prepared in 23.3% yield. Their compositions were determined by ESI-MS spectrometry (Figure S10), and the spectra show two fragment peaks at *m/z* = 2883.76 Da (calc. 2884.26 Da) and *m/z* = 2553.86 Da (calc. 2552.77 Da), corresponding to **$[2_H]^+$** and a species than can be formulated as $[AgCu_{12}\{S_2P(O^iPr)_2\}_6(C{\equiv}CPh)_4]^+$, respectively. This latter species can be described as resulting from a loss by **2** of two copper acetylide units and two hydrides (*vide infra*). The isotopic pattern of the observed cluster cation **2** shows good agreement with its simulated one (Figure S10: inset). Interestingly, the ESI-MS spectrum of **2_D** only shows a band at *m/z* 2554.33 Da, corresponding to the degradation of **2_D** via loss of two copper acetylides $[AgD_2Cu_{12}\{S_2P(O^iPr)_2\}_6(C{\equiv}CPh)_4]^+$ (calc. 2554.32 Da). Both simulated and experimental isotopic patterns match well (Figure S11: inset).

The ^1H NMR spectrum of **2_H** also shows a similar pattern as in **1**, one set of $C{\equiv}CPh^-$ and two sets of dtp isopropyl groups (Figure S13). The NMR spectrum suggests no two-fold symmetry imposed on the dtp ligand environment around the cluster core. The two hydrides of the linear $[AgH_2]^-$ embedded in the Cu_{14} cage are chemically and magnetically equivalent. Therefore, the hydride chemical shift centered at 5.15 ppm splits into two doublets ($^1J(^1H\text{-}^{107}Ag)$ = 93.6 Hz, $^1J(^1H\text{-}^{109}Ag)$ = 107.7 Hz) where a part of the signals is superimposed with the methine protons of the dtp ligands. The splitting pattern is further confirmed by its simulated ^1H NMR spectrum; that is the hydrides coupled with both ^{107}Ag and ^{109}Ag nuclei (Figure S14, Table S1). In addition, the ^{109}Ag NMR spectrum (Figure S15, Table S1) shows a triplet centered at 1279.5 ppm ($^1J(^1H\text{-}^{109}Ag)$ = 107.7 Hz) that echoes the scalar coupling constant observed in ^1H NMR spectrum. The presence of two hydrides in **2** is further confirmed by the ^2H NMR spectrum of its deuteride analogue (**2_D**), which shows a signal at 5.15 ppm ($^1J_{DAg}$ = 15.4 Hz) in THF at 297K, and its scalar coupling pattern can be fitted by a simulated spectrum of ($^1J(^2H\text{-}^{107}Ag)$ = 14.4 Hz, $^1J(^2H\text{-}^{109}Ag)$ = 16.5 Hz) (Figure S16, Table S2).

The brand-new bimetallic $[AuCu_{11}\{S_2P(O^iPr)_2\}_6(C{\equiv}CPh)_3Cl]$ (**3**) cluster, a two-electron superatom (*vide infra*), was prepared in 45% yield by adding one equiv. of $Au(PPh_3)Cl$ into an acetone solution of **H_2Cu_{11}** (Scheme 1). Its formation is concomitant with the liberation of H_2 gas (4.58 ppm), as the result of an internal redox reaction in which the hydride ligands of **H_2Cu_{11}** reduce Au(I) to Au(0). The chloride ion comes from the Au(I) salt. The composition of **3** determined by ESI-MS (Figure S19) shows a molecular ion peak at *m/z* 2478.43 (calc. 2478.40), corresponding to the loss of Cl^- by **3**, *i.e.* $[AuCu_{11}\{S_2P(O^iPr)_2\}_6(C{\equiv}CPh)_3]^+$. In addition, two higher molecular ion peaks also were observed at *m/z* 2543.37 (calc. 2541.33) and *m/z* 2642.40 (calc. 2642.37),

10.1002/anie.202113266

which can be reasonably formulated as [**3** + Cu - Cl]$^+$ and [**3** + {CuC≡CPh} - Cl]$^+$ (*vide infra.*), where their detected isotopic patterns are in good agreement with the simulation patterns (Figure S19: Inset).

The formations of **2** and **3** were also attempted via one-pot synthesis. This method failed to produce **2**, whereas **3** was formed at a very low yield (6.3%). These results emphasize the template effect of **H_2Cu_{11}** in the formation of compounds **1-3**.

Structure Analysis

Single crystals of **1**·**PF_6**, **2**·**PF_6**, and **3** suitable for diffraction analysis were grown in acetone/hexane (*v/v* = 1/2). Crystallographic data and selected interatomic distances are given in Table S3 and Table 1, respectively.[16]

As depicted in Figure 1a, the structure of **1** is strongly related to that of its **H_2Cu_{11}** precursor.[9] The latter template exhibits a Cu_{11} 3,3,4,4,4-pentacapped trigonal prism with the two hydrides located inside the top and bottom Cu_4 tetrahedra (μ_4-H), in a position closer to the prism triangular face, *i.e.* in a trigonal pyramidal coordination mode. The whole **H_2Cu_{11}** framework has D_{3h} ideal symmetry. The only significant difference between the **H_2Cu_{11}** precursor and **1** is that **1** has a supplementary Cu^+ ion inserted at the center of the pentacapped trigonal prism, thus right in the middle of the H…H axis, depicting a linear CuH_2 motif encapsulated within a Cu_{11} pentacapped triangular prism, the whole framework maintaining its D_{3h} ideal symmetry. Hence, the complete coordination environment of the two interstitial hydrides is now trigonal bipyramidal (μ_5-H), but with the averaged Cu_{top}-H (1.92(5) Å) and Cu_{tri}-H (2.00(5) Å) distances being significantly larger than Cu_{cent}-H (1.57(5) Å). When compared to their **H_2Cu_{11}** counterparts,[9] the Cu-Cu distances in **1** indicate that the insertion of one copper atom expands substantially the trigonal prismatic Cu_6 core. Beside of these differences, both **H_2Cu_{11}** and **1** have similar ligand environment, *i.e.* six dtp ligands that cap Cu_{top}-Cu_{tri}-Cu_{tri}-Cu_{cap} butterflies through a (μ_2, μ_2) binding mode and three triply-bridging alkynyl groups (μ_3-η^1) on the waist edge of the trigonal prism and one Cu_{cap} atom. The alkynyl groups are inclined in such a way that the whole cluster symmetry is lowered to C_{3h}.

The structure of the monocationic cluster **2** is shown in Figure 1c. The AgH_2Cu_{14} framework consists of an Ag-centered Cu_{12} icosahedron with two supplementary Cu atoms capping opposite faces (Figure 1d). The two hydrides are located on both sides of the central Ag atom, forming a linear AgH_2 motif along the Cu_{cap}....Cu_{cap} C_3 axis (Figure 1e). As depicted in Figure 1c, the AgH_2Cu_{14} framework (figure 1e), of D_{3d} ideal symmetry, is stabilized by six dtp and six alkynyl ligands. Each dtp ligand bridges four copper metals (one Cu_{cap} and three Cu_{ico}) in a (μ_2, μ_2) binding mode. The six alkynyl ligands are arranged along the waist of the copper icosahedron in a μ_3-η^1 fashion. As a result of the ligand arrangement, the whole cluster symmetry is lowered to

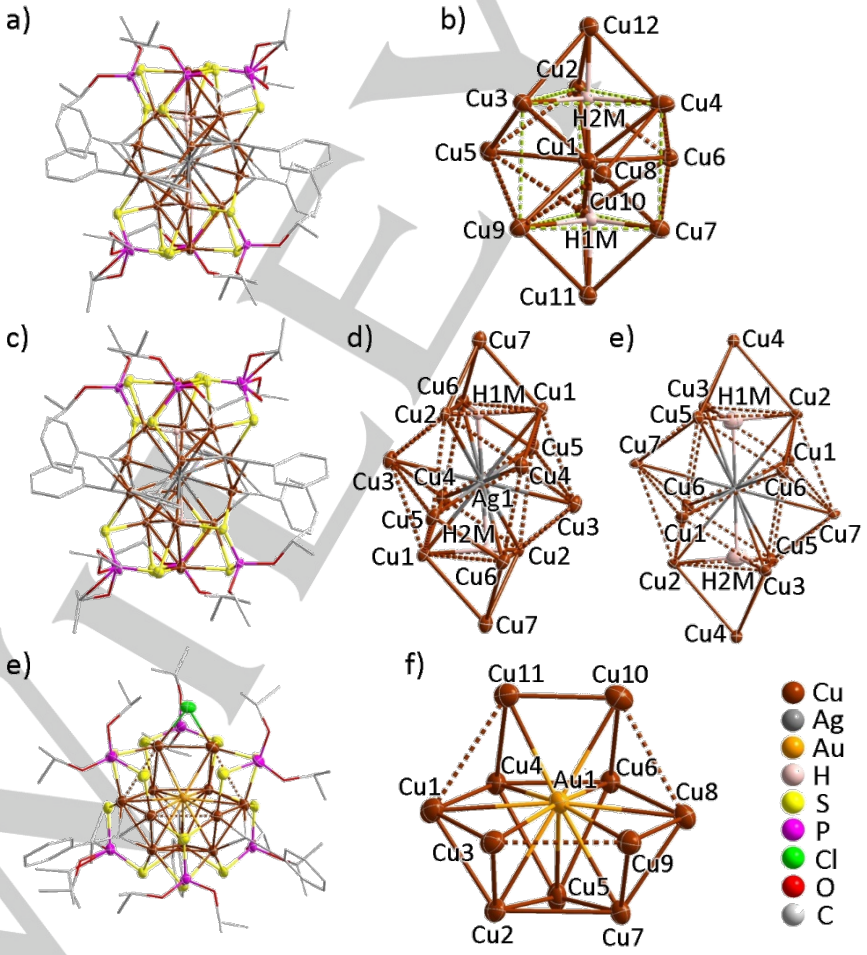

Figure 1. a) Total structure of **1**; b) The 3,3,4,4,4-trigonal prism geometry shell structure of **1** which houses a linear CuH_2 unit; c) The structure of cluster **2**; d) The Cu_{14} bicapped icosahedral framework of **2** which houses a linear AgH_2 unit; e) A view of the AgH_2Cu_{14} core of **2_N** showing a trigonal pyramidal hydride coordination mode for H1M atom; f) Total structure of **3** with H atoms omitted for clarity; g) The $AuCu_{11}$ core of **3**. (Thermal ellipsoids were drawn at the 50% probability level.)

Table 1. Selected interatomic distances (Å) for **1**, **2**, **3** (X-ray) and $\mathbf{2_N}$ (neutron).

Comp. /M_{cent}	M_{cent}-H	M_{cent}-Cu	Cu_{top}-H	Cu_{tri}-H	Cu_{ico}-H	Cu_{top}-Cu_{tri}	Cu_{tri}-Cu_{tri}[a]	Cu_{cap}-Cu_{ico}	Cu_{ico}-Cu_{ico}	Cu-S	Cu-C	C≡C	Cu-Cl
1 / Cu	1.51(5)-1.63(4) avg. 1.57(5)	2.5496(6)-2.6862(7) avg. 2.6069(6)	1.86(4)-1.97(5) avg. 1.92(5)	1.86(4)-2.13(5) avg. 2.00(5)	-	2.6555(6)-2.7778(6) avg. 2.7317(6)	3.3453(7)-3.5377(7) avg. 3.4633(7)	-	-	2.2801(9)-2.4045(9) avg. 2.3321(10)	1.907(4)-2.137(3) avg. 2.041(3)	1.201(5)-1.216(5) avg. 1.210(5)	-
2 / Ag	2.07(7)-2.102(10) avg. 2.09(5)	2.7823(7)-2.9086(7) avg. 2.8202(7)	-	-	1.73(8)-1.89(9) avg. 1.81(6)	-	-	2.7095(9)-2.7768(10) avg. 2.7417(9)	2.5833(9)-3.2255(8) avg. 2.971(1)	2.2560(17)-2.4659(15) avg. 2.3613(14)	1.915(5)-2.186(5) avg. 2.052(5)	1.214(7)-1.232(7) avg. 1.221(7)	-
$\mathbf{2_N}$ / Ag	1.950(11)-1.960(12) avg. 1.955(12)	2.759(3)-2.911(4) avg. 2.833(4)	-	-	1.780(11)-1.905(14) avg. 1.828(12)	-	-	2.712(6)-2.810(5) avg. 2.751(6)	2.635(5)-3.247(6) avg. 2.983(6)	2.265(10)-2.489(12) avg. 2.376(11)	1.921(5)-2.204(6) avg. 2.064(6)	1.227(7)-1.248(6) avg. 1.239(7)	-
3 / Au	-	2.7181(12)-3.1920(10) avg. 2.8869(9)	-		2.5319(15)-2.9413(12), avg. 2.7384(12)					2.275(2)-2.439(2) avg. 2.329(2)	1.978(7)-2.087(7) avg. 2.015(7)	1.227(7)-1.248(6) avg. 1.239(7)	2.368(3)-2.421(3) avg. 2.395(3)

[a] Egde distances within the triangular planes defining the Cu_6 trigonal prism.

S_6. A similar type of ligand-protected $MH_2@Cu_{14}$ (M = Cu and Pd) structure was previously observed in the isoelectronic clusters $[Cu_{15}H_2\{S_2CNR_2\}_6(C{\equiv}CPh)_6](PF_6)$[10] and $[PdH_2Cu_{14}\{dtc/dtp\}_6(C{\equiv}CPh)_6]$.[12] The two interstitial hydrides have been unequivocally characterized by single-crystal neutron crystallography (structure $\mathbf{2_N}$, Figure 1e). Interestingly, the two hydrides were found to be in a 4-coordinated (μ_4) trigonal pyramidal geometry instead of the trigonal bipyramidal geometry observed in both $[CuH_2Cu_{14}(dtc)_6(C{\equiv}CPh)_6]^+$ [10] and $[PdH_2Cu_{14}(dtc)_6(C{\equiv}CPh)_6]$.[12] Indeed, The Cu_{cap}...H distances (avg. 2.31(1) Å) in $\mathbf{2_N}$, indicate clearly no significant contacts between these two atoms, whereas The Cu_{ico}-H and Ag-H distances in $\mathbf{2_N}$ are much shorter (avg. 1.828(12) and 1.955(12) Å, respectively). On the contrary, the Cu_{cap}...H distances are much shorter in the neutron structures of $[CuH_2Cu_{14}(dtc)_6(C{\equiv}CPh)_6]^+$ (2.020(16) Å)[10] and $[PdH_2Cu_{14}(dtc)_6(C{\equiv}CPh)_6]$ (1.863(5) Å).[12] This difference can be attributed to the different bite distances between the dtc and dtp ligands. The bite distance of the dtp ligand in **2** is 3.44 Å. That of the dtc ligand is shorter: 3.05 Å in $[CuH_2Cu_{14}(dtc)_6(C \equiv CPh)_6]^+$,[10] and $[PdH_2Cu_{14}(dtc)_6(C \equiv CPh)_6]$.[12] Since these ligands are bridging the Cu_{cap} and Cu_{ico} atoms, their bite distance directly influences the Cu_{cap}…Cu_{ico} distances, and by implication the Cu_{cap}…H distance. The Ag_{cent}-H-Cu_{tri} and Cu_{tri}-H-Cu_{tri} angles in **2** (avg. 97.4(5)° and 118.3(5)°, respectively), also reflect the hydride trigonal pyramidal coordination mode. To the best of our knowledge, *this is the first example of a neutron-characterized trigonal pyramidal hydride coordination mode in a $AgCu_3$ environment, coming right after that in a Cu_4 environment, also proven to exist by neutron diffraction in* $\mathbf{H_2Cu_{11}}$.[9]

It is worthwhile to mention that the trigonal pyramidal hydride coordination mode observed in **2** is one among several other μ_4-H possibilities.[1a,7,17] Finally, a question that arises then is why, when treated with Cu^+, $\mathbf{H_2Cu_{11}}$ leads to the formation of **1** ($CuH_2@Cu_{11}$), whereas when treated with Ag^+, **2** ($AgH_2@Cu_{14}$) is formed. The answer is likely to be a size effect, the linear AgH_2 unit being too large to accommodate within the rigid trigonal prismatic Cu_6 central core that exists in **1**. This assumption is confirmed by our DFT results (*vide infra*).

The structure of **3** is shown in Figure 1f. The metal core of $AuCu_{11}$ (Figure 1g) can be viewed as an Au-centered Cu_{12} cuboctahedron with one missing vertex. In that respect, it is related to $[AuCu_{12}\{S_2CN^nBu_2\}_6(C{\equiv}CPh)_4]^+$,[11] and $[AuCu_{12}\{S_2P(O^iPr)_2\}_6(C{\equiv}CPh)_4]^+$ (**4**),[13] which display a complete cuboctahedral $Au@Cu_{12}$ metal core protected by six dtc/dtp ligands bridging the six square faces in a (μ_2, μ_2) mode and four alkynyl ligands capping half of the triangular faces in a (μ_3-η^1) fashion. Removal of one Cu^+ vertex in these species causes two dtp ligands switching to (μ_2, μ_1), whereas the four others remain (μ_2, μ_2). Three alkynyls in **3** adopt similar (μ_3-η^1) bridging mode as those in $[AuCu_{12}\{S_2CN^nBu_2\}_6(C{\equiv}CPh)_4]^+$ and **4**, but the fourth alkynyl in the latter is replaced by a chloride ligand in **3**, which bridges the (no more triangular) Cu10-Cu11 edge (Figure 1f). The Au-Cu and Cu-Cu distances are comparable to those found in $[AuCu_{12}\{S_2CN^nBu_2\}_6(C{\equiv}CPh)_4]^+$,[11] and in **4**.[13] The $Au@Cu_{12}$ cuboctahedral metal core can be seen as the simplest unit of bulk fcc. The $Au@Cu_{11}$ core in **3** can then be visualized as a vacancy-defect *fcc* structure (Scheme 2). Not only **3** is structurally related to the cuboctahedral **4**, but there is also an electronic relationship between them, as, with a $[AuCu_{11}]^{10+}$ metal core for the former and $[AuCu_{12}]^{11+}$ for the latter,[11] they both can be described as 2-electron superatoms (*vide infra*).[11]

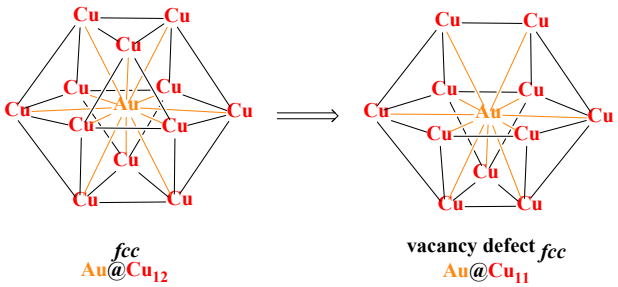

Scheme 2. An illustration of the complete *fcc* structure of **4** with the *fcc* vacancy defect structure of the metal core in **3**.

Optical and Photoluminescence (PL) Properties

The UV-Vis absorption spectra of clusters **1**, **2**, and **3** are shown in Figure 2a. The homometallic cluster **1** exhibits two optical absorption peaks with an intense peak at 347 nm and a broad shoulder band at 423 nm. It is almost identical to that of $\mathbf{H_2Cu_{11}}$ (Figure S23). Thus, insertion of a Cu atom at the center of the

10.1002/anie.202113266

H_2Cu_{11} cage does not significantly affect the optical properties. On the other hand, the spectrum of cluster **2** shows a distinct absorption pattern, with a weak shoulder at 417 nm. In sharp contrast to **1** and **2**, the optical spectrum of cluster **3** exhibits a multiband absorption profile, a typical feature for superatom-type clusters, centered at 432, 483, 540 nm and an intense absorption band at 328 nm.

Similarly, as its **H_2Cu_{11}** template, **1** is not emissive. The Ag-doped cluster **2** luminesces, but only at 77K. Its emission spectrum (λ_{ex} = 464 nm) shows a broad structureless band centered at 642 nm (Figure 2b). On the other hand, **3** exhibits an intense orange-red emission centered at 606 nm in MeTHF at both ambient and liquid nitrogen temperatures. The PL intensity at 77 K is six times stronger than that at ambient temperature (Figure 2b and S24a). The excitation spectrum of **3** monitored at 606 nm is almost identical to its absorption spectrum (Figures 2b, S24b and S24c). The room-temperature quantum yield (QY) is found to be 3.3% with a lifetime of 3.75 µs (Figure S25), an indicator of a triplet excited state. The room temperature QY of **3** is significantly higher than that of the other two clusters, which do not emit at ambient temperature.

Both **3** and **4**[13] have distinct photophysical properties. The emission band of **3** centered at 606 nm red-shifts to 637 nm in the case of **4**, accompanied with a two-fold increase of PL intensity (Figure S26). Besides, the QY of **4** (32%) is ten times higher than that of **3** (3.3%). The lower PL intensity and QY of **3** may be ascribed to a less rigid copper framework due to the vacancy defect. In addition, the radiative rate constant (k_{RAD}) of **4** is about 11 times larger than that of cluster **3,** whereas the non-radiative rate constant (k_{NRD}) of **4** is similar to that of cluster **3** (0.21 *vs.* 0.26 μs^{-1}) (Table S3). Hence the much larger QY of **4** is consistent with the larger value of k_{RAD} in **4** compared to **3**.

Stability

The stability of **1** in dichloromethane at ambient temperature was monitored by UV-Vis spectrometry. The two absorption bands of **1** change steadily over time, indicating complete decomposition in 5 days (Figure S27). Further, the stability of **1** was investigated by variable temperature ^{1}H and ^{31}P{^{1}H} NMR (30 to 55°C) in *d*$_6$-acetone (Figure S28 and S29). The results indicate that raising temperature leads to the decomposition of **1** to $[Cu_8H\{S_2P(O^iPr)_2\}_6]^+$,[18] conversion of the alkynyl ligands to styrene, with ^{1}H NMR resonances in the range 5.20-7.13 ppm, and liberation of H_2 (4.53 ppm). At higher temperature, the ^{31}P NMR spectrum of **1,** which resonates at 99.5 ppm, shifts downfield to 100.4 ppm, which is the resonance frequency of $[Cu_8H\{S_2P(O^iPr)_2\}_6]^+$. Based on these observations, one can conclude that, at an elevated temperature (55°C), cluster **1** is not as stable as its precursor template, **H_2Cu_{11}**.[9] In fact its purification is quite challenging. **1** decomposes into the starting **H_2Cu_{11}** template when passing through an aluminium oxide chromatography column.

The degradation of **2** was investigated by time-dependent ^{1}H and ^{31}P{^{1}H} NMR spectroscopy in $CDCl_3$ (Figure S30). It leads to the formation of the 2-electron bimetallic cluster $[AgCu_{12}\{S_2P(O^iPr)_2\}_6(C{\equiv}CPh)_4]^+$ (**5**) with liberation of H_2 (4.62 ppm). Indeed, the ^{1}H NMR chemical shifts of the alkyl groups characteristics of **2** coalesce steadily over time and show good agreement with the chemical shifts of the alkyl groups in **5** (Figure S31). Consistently, the ^{31}P{^{1}H} NMR resonance frequency of **2** (101.2 ppm (Figure S32) shifts upfield to 100.5 ppm, the chemical shift of **5** (Figure S33). This is also supported by the ESI-MS spectrometry as depicted in Figure S34. Thus, during the degradation, the two hydride ligands are oxidized to H_2, reducing formally Ag(I) to Ag(0) through an internal redox reaction,[19] accompanied by the rearrangement of the core structure from bicapped icosahedral ($AgH_2@Cu_{14}$) to cuboctahedral ($Ag@Cu_{12}$) and successive loss of two copper acetylide units. The degradation was further observed by using UV-Vis spectroscopy in CH_2Cl_2 under daylight (Figures S35 and S36), which indicates that cluster **2** collapses into cluster **5** within 24 hours. When the same experiment is performed in the dark, cluster **2** can survive for several days and degrades more slowly (Figures S37 and S38). We propose the degradation process of **2** to **5** shown in Scheme S1. Furthermore, the reaction of a 1:1 mixture of $Cu_{11}H_2$ and $Cu_{11}D_2$ with Ag(I) was conducted and monitored through NMR spectroscopy, which only showed the presence of the corresponding hydride or deuteride peak for **2**, without any scrambling of the hydride ligands (Figures S47-48).

Time-dependent ^{1}H and ^{31}P{^{1}H} NMR spectroscopy of **3** in $CDCl_3$ (Figures S39 and S40) show it evolves into the previously reported 2-electron bimetallic **4**,[13] through a partial aggregation process. Indeed, the two sets of ^{1}H chemical shifts of the dtp alkyl groups in **3** merge into one set in **4**. This result is further confirmed

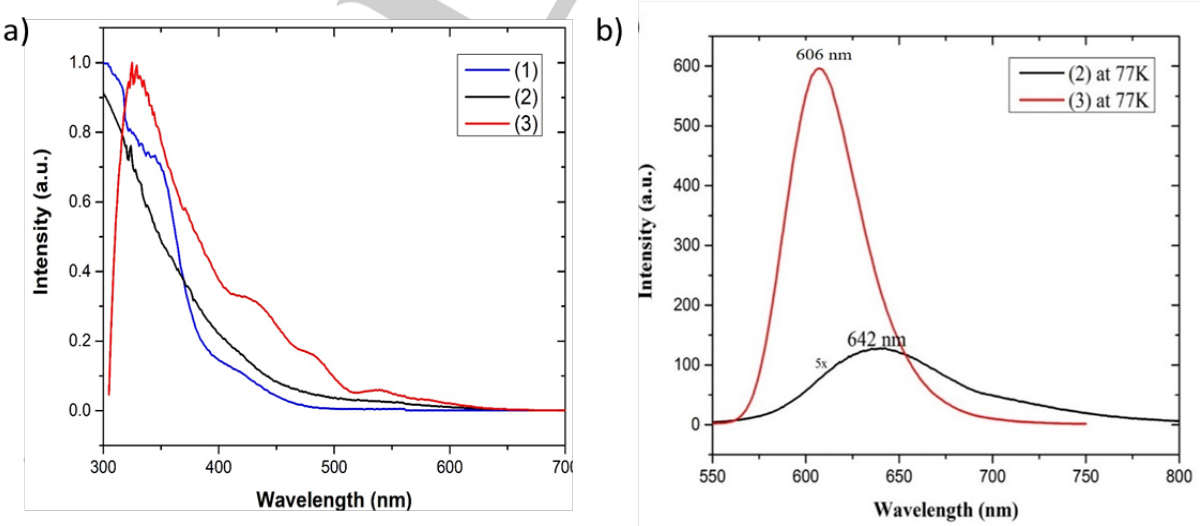

Figure 2. a) The absorption spectra of **1**, **2**, and **3** in dichloromethane ($1.07x10^{-5}$ M). b) Emission spectra of **2** and **3** in 2-MeTHF at 77K.

by the $^{31}P\{^{1}H\}$ NMR spectra recorded at ambient temperature, in which the $^{31}P\{^{1}H\}$ NMR resonance at 97.8 ppm, the chemical shift of **3** shifts within a day, to 101.7 ppm, the chemical shift of **4**. Importantly the alloy **4** can be isolated in 46.9% yield from the reaction of compound **3** with one equiv. of [CuC≡CPh] (Scheme S2, Figures S42 and S43). Thus, the less stable **3**, which has an incomplete cuboctahedral copper core, evolves to the perfect *fcc* metal arrangement of **4**. This observation was also supported by ESI-MS that shows the presence of each fragment (Figure S41). We thus propose **3** to be a key precursor in the formation of the more stable cluster **4** , which is not directly produced from **$Cu_{11}H_2$** in the Scheme 1 reaction conditions, *driven by the structure transition from defect fcc to complete fcc*.

Theoretical analysis

DFT and TD-DFT calculations were carried out at the PBE0/Def2-TZVP (see Computational Details in the SI) on model of clusters **$Cu_{11}H_2$** and **1-3** in which the dtp ligands were simplified in S2PH2 ligands. These models are named **$Cu_{11}H_2$'**and **1'-3'** in the followings. Their optimized structures (see SI) are in an overall good agreement with their experimental counterparts. Selected computed data are given in Table 2. The Cu-H distances computed for **1'** are in a quite satisfying agreement with the X-ray structure of **1**, owing to the moderate accuracy of the latter. They confirm the hydride trigonal bipyramidal coordination mode. The computed Cu_{cent}-H distance (1.638 Å) is short and approaches that of the free linear $[CuH_2]^-$ ion (1.571 Å) computed at the same level. Consistently, the corresponding Wiberg bond index (WBI) (0.217) is much larger than the other Cu-H WBIs. Clearly, the $Cu_{cent}H_2$ unit in **1'** can be considered as a $[CuH_2]^-$ 14-electron complex (a stable electron configuration) encapsulated within a ligated $[Cu_{11}]^{11+}$ cage. The $Cu_{cent}H_2$ NAO charge (-0.88) is indicative of a small electron transfer towards the cage, the interaction between the cage and its host being largely of ionic character. Nevertheless, the Cu and hydride NAO charges of **1'** remain quite similar to that found in **$Cu_{11}H_2$'**.

The Ag_{cent} -H and Cu_{ico}-H distances computed for **2'** are in a very good agreement with the neutron structure **2_N**. Although somewhat shorter, the computed Cu_{cap}-H distance (2.028 Å) is not significantly different (at 3σ) from its neutron counterpart (2.31 Å). In any case, the optimized Cu_{cap}-H distance is large and its WBI small. Similarly, as in **1'**, the data computed for **2'** (Table S5) are consistent with the view of a 14-electron linear $[Ag_{cent}H_2]^-$ complex encapsulated within a bicapped icosahedral $[Cu_{14}]^{14+}$ ligated cage. The encapsulated $[Ag_{cent}H_2]^-$ unit is more elongated in **2'** than the $[Cu_{cent}H_2]^-$ unit in **1'** (17% *vs.* 4%) and its NAO charge (-1.22) overpasses that of the free d^{10} complex (-1). This is the trace of a somewhat counterintuitive electron transfer from the cage 3d(Cu) AOs into the empty $5p_\pi$(Ag) ones, which largely overpasses the weak transfer from the hydrides to the 4s AOs of Cu_{tri} and (if any) Cu_{cap}. Thus, the $[M_{cent}H_2]^-$ identity of the encapsulated unit is less marked in **2'** than in **1'**. Although larger by ~ 1 ppm than the experimental hydride chemical shifts of **$Cu_{11}H_2$**,[9] **1** and **2** (4.89, 5.24 and 5.15 ppm, respectively), those computed in vacuum for **$Cu_{11}H_2$'**, **1'** and **2'** (5.9, 6.2 and 6.2 ppm, respectively) reflect their variation nicely.

The question that arises now is why treating **$Cu_{11}H_2$** with Ag^+ or with Cu^+ leads to compounds (**2** and **1**, see Scheme 1) of different structures and, overall, global compositions. To answer these questions, we calculated models of **1** and **2** in which the encapsulated metal is substituted by Ag and Cu, respectively.

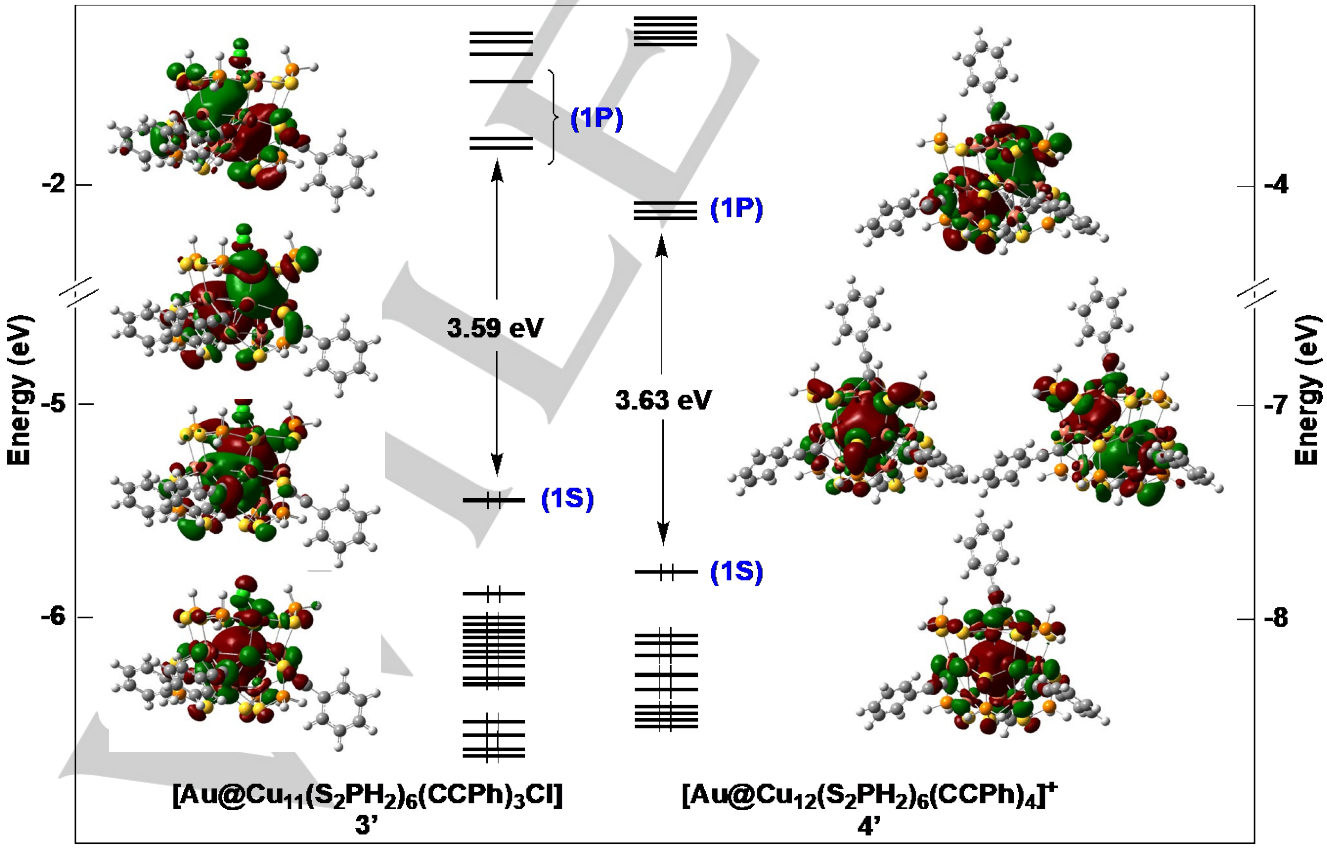

Figure 3. The Kohn-Sham frontier orbital diagrams of **3'** and **4'**.

These new models are called **1(Ag)'** and **2(Cu)'**, respectively. It turned out that the geometry of **1(Ag)'** was particularly hard to converge, a sign of instability. The geometry that we obtained (see SI) is highly distorted and does not reflect at all the topology of **1'**. Thus, the ligated Cu_{11} cage of **1** is too small and not flexible enough for letting an Ag atom substituting Cu_{cent}. On the other hand, the larger ligated Cu_{14} cage in **2** provides enough space for the $[Ag_{cent}H_2]^-$ unit to expand its size by 17%. Contrarily to **1(Ag)'**, **2(Cu)'** easily converged to a structure similar to that of **2** (Table S5). These results are consistent with a cage size effect which favors the formation of **1** with Cu^+ and that of **2** with $\mathbf{Ag^+}$ (Scheme 1). Although the formation of **2(Cu)** is not observed in our reaction conditions, our DFT results do not exclude its isolation in different conditions, despite its expected lower chemical stability. On the other hand, the existence of **1(Ag)** should be discarded.

Selected data computed for of **3'** and **4'** are gathered in Table 2. Their optimized geometries (see SI) match satisfyingly the X-ray structures of **3** and **4**.[13] Both **3'** and **4'** structures have similar metrics, the Cu-Cu distances of **3'** being slightly shorter than those of **4'**, due to some shrinking of the vertex-missing cuboctahedron.Their NBO charge distribution are also quite similar. It is of note that the Au charge is neatly negative, whereas that of the Cu atoms are of the same order of magnitude as than in the Cu(I) hydrides of Table S5. The Au-Cu and Cu-Cu WBIs are rather small, suggesting little electron sharing between metals, thus a limit view of Au(0) and Cu(I); in other word, a 2-electron superatoms with dominant localization of the superatomic 1S orbital on Au. This is supported by the MO diagrams of **3'** and **4'** (Figure 3), which show a gold-polarized 1S HOMO and three lowest unoccupied orbitals that can be identified as the 1P level. The electronic structure of the *fcc* vacancy defect structure of **3** is thus strongly related to that of the complete *fcc* structure of **4**. This relationship is reminiscent of the *nido*/*closo* parentage in the well-known family of the Wade-Mingos clusters.[20]

Table 2. Table Caption Selected DFT-computed data for **3'** and **4'** models.

		3'	**4'**
HOMO-LUMI gap (eV)		3.59	3.63
Interatomic distances (Å) and Wiberg indices (avg. values)	Au-Cu	2.814 [0.060]	2.821 [0.054]
	Cu-Cu	2.789 [0.041]	2.818 [0.038]
NAO charges (avg. values)	Au	-0.73	-0.81
	Cu	0.72	0.74

The TDDFT-simulated spectra of **1'**, **2'** and **3'** are shown in Figure S44. The intense peak recorded at 347 nm for **1** is reproduced at 357 nm for **1'**. It can be assigned to a HOMO-1→LUMO+1 transition, with mixed MLCT/M(3d)M(4s)CT character. The weak band recorded for **1** at 423 nm is not reproduced for **1'**. The weak shoulder around 417 nm observed for **2** appears around 390 nm in the simulated spectrum of **2'**, resulting from transitions of M(Cu)LCT nature. The broad low energy band around 350 nm appearing in the simulated spectrum of **3'** results from HOMO→LUMO and HOMO→LUMO+1 transitions, hence of superatomic 1S→1P nature.

Conclusion

The copper(I) dihydride cluster $[Cu_{11}H_2\{S_2P(O^iPr)_2\}_6(C{\equiv}CPh)_3]$ (**H_2Cu_{11}**) template generates a surprisingly rich chemistry when exposed to reactions with M^+ (M = Cu, Ag, Au) ions. Depending on the nature of M, three different (non-isostructural, non-isoelectronic) clusters are formed. Both **1** and **2** are Cu(I) or Cu(I)/Ag(I) species and maintain the same number of hydride ligands as their **H_2Cu_{11}** precursor. However, whereas **1** results from the simple insertion of a Cu^+ ion right at the center of the **H_2Cu_{11}** core, with the formation of an encapsulated $[CuH_2]^-$ linear unit within a pentacapped trigonal prismatic $[Cu_{11}]^{11+}$ cage, a different structure is obtained with the larger Ag^+ ion which provokes the collapse of the pentacapped trigonal prismatic cage of **H_2Cu_{11}**. The resulting cluster **2** contains also a 14-electron linear encapsulated $[AgH_2]^-$ unit, but this time encapsulated in a $[Cu_{14}]^{14+}$ cage of bicapped icosahedral configuration. Contrarily to the Cu^+ and Ag^+ cases, the treatment of **H_2Cu_{11}** with Au^+ does not lead to a hydrido species, but to cluster **3**, which has a partly reduced $[AuCu_{11}]^{10+}$ metal core, and thus is a 2-electron superatom related to **4**. The core of **3** can be viewed as a *defect fcc* structure related to the complete *fcc* core of the more stable cluster **4**. Thus, depending on the nature of M^+, the hydride ligands in **H_2Cu_{11}** play a different role. With Cu^+ and Ag^+ they act as ligands and stabilize $[MH_2]^-$ 14-electron complexes that are encapsulated in $[Cu_n]^{n+}$ cages. In the case of Au^+, they act as reducing agents, leading to the formation of a 2-electron superatom, with liberation of H_2. Degradation of **2** and partial aggregation of **3** in solution lead to the formation of bimetallic clusters **5** and **4**, respectively. With a complete cuboctahedral (*fcc*) $M@Cu_{12}$ (M = Ag, Au) metal core, such 2-electron superatomic frameworks appear to be thermodynamical sinks in this chemistry. Furthermore, the **H_2Cu_{11}** template presents possibilities in catalytic formic acid (FA) dehydrogenation reactions, which potentially liberate H_2 and CO_2, and cluster **1** as byproducts. These results will be reported soon.

Acknowledgements

This work was supported by the Ministry of Science and Technology of Taiwan (MOST, Grant No.109-2113-M-259-008), the France-Taiwan ANR-MOST program (project Nanoalloys) and the GENCI computing resource (grant A0090807367). Q. W. thanks the China Scholarship Council for a Ph.D. grant. The single-crystal neutron diffraction measurements performed on TOPAZ used resources at the Spallation Neutron Source, a DOE Office of Science User Facility operated by the Oak Ridge National Laboratory.

Keywords: hydride • copper • gold • silver • neutron diffraction

[1] a) R. S. Dhayal, W. E. van Zyl, C. W. Liu, *Acc. Chem. Res.* **2016**, *49*, 86–95; b) A. J. Jordan, G. Lalic, J. P. Sadighi, *Chem. Rev.* **2016**, *116*, 8318–8372; c) R. S. Dhayal, W. E. van Zyl, C. W. Liu, *Dalton Trans.* **2019**, *48*, 3531–3538; d) T. Nakajima, K. Nakamae, Y. Ura, T. Tanase, *Eur. J. Inorg. Chem.* **2020**, 2211-2226; e) C. Sun, B. K. Teo, C. Deng, J. Lin, G. -G. Luo, C. -H. Tung, D. Sun, *Coord. Chem. Rev.* **2021**, 427, 213576.

[2] a) R. S. Dhayal, J. -H. Liao, L. -R. Lin, P. -K. Liao, S. Kahlal, J. -Y. Saillard, C. W. Liu, *J. Am. Chem. Soc.* **2013**, *135*, 4704–4707; b) C. Sun, N. Mammen, S. Kaappa, P. Yuan, G. Deng, C. Zhao, J. Yan, S. Malola, K. Honkala, H. Hakkinen, B. K. Teo, N. Zheng, *A.C.S. Nano.* **2019**, *13*,

5975–5986; c) T. Nakajima, Y. Kamiryo, M. Kishimoto, K. Imai, K. Nakamae, Y. Ura, T. Tanase, *J. Am. Chem. Soc.* **2019**, *141*, 8732–8736; d) R. Huang, J. Yin, C. Dong, A. Ghosh, M. J. Alhilaly, X. Dong, M. N. Hedhili, E. Abou-Hamad, B. Alamer, S. Nematulloev, Y. Han, O. F. Mohammed, O. M. Bakr, *J. Am. Chem. Soc.* **2020**, *142*, 8696; e) A. Chen, X. Kang, S. Jin, W. Du, S. Wang, M. Zhu, *J. Phys. Chem. Lett.* **2019**, *10*, 6124-6128; (f) S. Takano, H. Hirai, S. Muramatsu, T. Tsukuda, *J. Am. Chem. Soc.* **2018**, *140*, 8380-8383.

[3] a) Q. Tang, Y. Lee, D. -Y. Li, W. Choi, C. W. Liu, D. Lee, D. -E. Jiang, *J. Am. Chem. Soc.* **2017**, *139*, 9728–9736; b) Y. Li, H. Z. Ma, G. E. Reid, A. J. Edwards, Y. Hong, J. M. White, R. J. Mulder, R. A. J. O'Hair, *Chem. – Eur. J.* **2018**, 24, 2070–2074; c) S. Lee, M. S. Bootharaju, G. Deng, S. Malola, W. Baek, H. Hakkinen. N. Zheng, T. Hyeon, *J. Am. Chem. Soc.* **2020**, *142*, 13974-13981; d) D. A. Ekanayake, A. Chakraborty, J. A. Krause, H. Guan, *Inorg. Chem. Front.* **2021**, 8, 4634-4649.

[4] P. -K. Liao, C. -S. Fang, A. J. Edwards, S. Kahlal, J. -Y. Saillard, C. W. Liu, *Inorg. Chem.* **2012**, *51*, 6577–6591.

[5] A. J. Edwards, R. S. Dhayal, P. -K. Liao, J. -H. Liao, M. -H. Chiang, R. O. Piltz, S. Kahlal, J. -Y. Saillard, C. W. Liu, *Angew. Chem. Int. Ed.* **2014**, *53*, 7214–7218; *Angew. Chem. 126*, 7342-7346.

[6] a) J. -H. Liao, R. S. Dhayal, X. Wang, S. Kahlal, J. -Y. Saillard, C. W. Liu, *Inorg. Chem*. 2014, *53*, 11140–11145; b) R. S. Dhayal, J. -H. Liao, X. Wang, Y. -C. Liu, M. -H. Chiang, S. Kahlal, J. -Y. Saillard, C. W. Liu, *Angew. Chem. Int. Ed.* **2015**, *54*, 13604-13608; *Angew. Chem. 127*, 13808-13812.

[7] S. K. Barik, S. -C. Huo, C. -Y. Wu, T. -H. Chiu, J. -H. Liao, X. Wang, S. Kahlal, J. -Y. Saillard, C. W. Liu, *Chem. – Eur. J.* **2020**, *26*, 10471–10479.

[8] R. S, Dhayal, J. -H. Liao, S. Kahlal, X. Wang, Y. -C. Liu, M. -H. Chiang, W. E. van Zyl, J. -Y. Saillard, C. W. Liu, *Chem. – Eur. J.* **2015**, *21*, 8369–8374.

[9] R. P. B. Silalahi, G. -R. Huang, J. -H. Liao, T. -H. Chiu, K. K. Chakrahari, X. Wang, J. Cartron, S. Kahlal, J. -Y. Saillard, C. W. Liu, *Inorg. Chem.* **2020**. *59*. 2536–2547.

[10] K. K. Chakrahari, J. Liao, R. P. B. Silalahi, T. -H. Chiu, J. -H. Liao, X. Wang, S. Kahlal, J. -Y. Saillard, C. W. Liu, *Small* **2021**, *17*, 2002544.

[11] R. P. B. Silalahi, K. K. Chakrahari, J. -H. Liao, S. Kahlal, Y. -C. Liu, M. -H. Chiang, J. -Y. Saillard, C. W. Liu, *Chem. Asian J.* **2018**, *13*, 500–504.

[12] K. K. Chakrahari, R. P. B. Silalahi, T. -H. Chiu, X. Wang, N. Azrou, S. Kahlal, Y. -C. Liu, M. -H. Chiang, J. -Y. Saillard, C. W. Liu, *Angew. Chem. Int. Ed.* **2019**, *58*, 4943–4947*; Angew. Chem. 131*, 4997-5001.

[13] R. P. B. Silalahi, T. -H. Chiu, J. -H. Kao, C. -Y. Wu, C. -W. Yin, Y. -C. Liu, Y. J. Chen. J. -Y. Saillard, M. -H. Chiang, C. W. Liu, *Inorg. Chem.* **2021**, 60, 10799–10807.

[14] a) E. Gottlieb, H. Qian, R. Jin, *Chem. –Eur. J.* **2013**, *19*, 4238–4243; b) S. Wang, Y. Song, S. Jin, X. Liu, J. Zhang, Y. Pei, X. Meng, M. Chen, P. Li, M. Zhu, *J. Am. Chem. Soc.* **2015**, *137*, 4018–4021; c) S. Yang, J. Chai, Y. Song, J. Fan, T. Chen, S. Wang, H. Yu, H. Li, M. Zhu, *J. Am. Chem. Soc.* **2017**, *139,* 5668–5671; d) Y. Niihori, M. Eguro, A. Kato, S. Sharma, B. Kumar, W. Kurashige, K. Nobusada, Y. Negishi, *J. Phys. Chem. C*. **2016**, *120*, 14301–14309; e) S. Yamazoe, W. Kurashige, K. Nobusada, Y. Negishi, T. Tsukuda, *J. Phys. Chem. C*. 2014, *118*, 25284–25290; f) X. Kang, Y. Li, M. Zhu, R. Jin, *Chem. Soc. Rev.* **2020**, *49*, 6443-6514; g) T. Kawawaki, Y. Imai, D. Suzuki, S. Kato, I. Kobayashi, T. Suzuki, R. Kaneko, S. Hossain, Y. Negishi, *Chem. -Eur. J.* **2020**, *26*, 16150-16193; h) A. G. Walsh, P. Zhang, *Adv. Mater. Interfaces*. **2021**, *8*, 2001342; i) Y. Du, H. sheng, D. Astruc, M. Zhu, *Chem. Rev.* **2020**, *120*, 526-622; j) S. Hossain, Y. Niihori, L. V. Nair, B. Kumar, W. Kurashige, Y. Negishi, *Acc. Chem. Res.* **2018**, *51*, 3114-3124.

[15] a) A. Albinati, L. M. Venanzi, *Coord. Chem. Rev.* **2000**, *200-202,* 687-715; b) A. Albinati, S. Chaloupka, F. Demartin, T. F. Koetzle, H. Ruegger, L. M. Venanzi, M. K. Wolfer, *J. Am. Chem. Soc.* **1993**, *115*, 169-175; c) M. Gorol, N. Mösch-Zanetti, H. W. Roesky, M. Noltemeyer, H. -G. Schmidt, *Chem. Commun.* **2003**, 46-47; d) D. Donghi, D. Maggioni, G. D'Alfonso, T. Beringhelli, *J. Organmet. Chem.* **2014**, *751*, 462-470; e) A. Hicken, A. J. P. White, M. R. Crimmin, *Angew. Chem. Int. Ed.* **2017**, *56*, 15127-15130; *Angew. Chem. 129*, 15323-15326; f) A. Hicken, A. J. P. White, M. R. Crimmin, *Dalton Trans.* **2018**, *47*, 10595-10600.

[16] Deposition number 2095375 (**1**), 2095376 (**2·PF$_6$**), and 2095378 (**3·PF$_6$**) contain the supplementary X-ray crystallographic data, and 2095377 (**2$_N$**) contains the neutron crystallographic data for this paper. These data are provided free of charge by the joint Cambridge Crystallographic Data Centre.

[17] a) Y. -J. Zhong, J. -H. Liao, T. -H. Chiu, Y. -Y. Wu, S. Kahlal, J. -Y. Saillard, C. W. Liu, *Chem. Commun.* **2020**, *56*, 9300–9303; b) Y. -J. Zhong, J. -H. Liao, T. -H. Chiu, Y. -Y. Wu, S. Kahlal, M. J. McGlinchey, J. -Y. Saillard, C. W. Liu, *Dalton Trans.* **2021**, *50*, 4727–4734

[18] a) P. -K. Liao, B. Sarkar, H. -W. Chang, J. -C. Wang, C. W. Liu, *Inorg. Chem.* **2009**, 48, 4089–4097; b) P. -K. Liao, K. -G. Liu, C. -S. Fang, C. W. Liu, J. P. Jr. Fackler, Y. -Y. Wu, *Inorg. Chem.* **2011**, 50, 8410–8417.

[19] Y. -J. Zhong, J. -H. Liao, T. -H. Chiu, S. Kahlal, C. -J. Lin, J. -Y. Saillard, C. W. Liu, *Angew. Chem. Int. Ed.* **2021**, *60*, 12712–12716; *Angew. Chem. 133*, 12822-12826.

[20] D. M. P. Mingos, D. J. Wales, (1990) Introduction to cluster chemistry. Prentice-Hall, Englewood Cliffs.

10.1002/anie.202113266

WILEY-VCH

RESEARCH ARTICLE

Entry for the Table of Contents

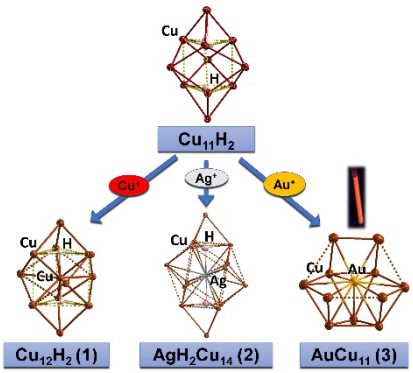

While the reaction of the $[Cu_{11}H_2\{S_2P(O^iPr)_2\}_6(C{\equiv}CPh)_3]$ template with Cu^+ or Ag^+ produces **$Cu_{12}H_2$** and Ag**$Cu_{14}H_2$** species in which the hydrides behave as Lewis bases, in the reaction with Au^+, the hydrides act as reducing agents, leading to a luminescent, 2-e $Au@Cu_{11}$ superatom, whose metal core has a defect *fcc* structure.